ISSN 0016-7932, Geomagnetism and Aeronomy, 2015, Vol. 55, No. 8, pp. 1104–1111. © Pleiades Publishing, Ltd., 2015.

Influence of Magnetic Turbulence on the Propagation of Accelerated Electrons and Hard X-Ray Brightness Distribution in Solar Flares

Yu. E. Charikov[a, b] and A. N. Shabalin[a]

[a] *Ioffe Physical-Technical Institute, Russian Academy of Sciences, Politekhnicheskaya ul. 26, St. Petersburg, 194021 Russia*

[b] *St. Petersburg State Polytechnical University, Politekhnicheskaya ul. 29, St. Petersburg, 195251 Russia*

e-mail: Y.Charikov@yandex.ru, taoastronomer@gmail.com

Received February 11, 2015; in final form, March 25, 2015

Abstract—The influence of magnetic turbulence on the hard X-ray brightness distribution in magnetic loops during solar flares was studied. An analysis was perfomed based on the solution of the kinetic equation for relativistic electrons, in which the regular energy loss, Coulomb scattering, magnetic reflection, and the effect of the reverse current and magnetic turbulence are taken into account. It was shown that scattering by magnetic inhomogeneities with parameter $\eta = \delta B/B = 10^{-3}$ results in an increase in hard X-ray brightness at loop footpoints when the distribution of accelerated electrons is isotropic and mostly in the loop coronal part if the electron source is anisotropic. The influence of magnetic turbulence is absent at $\delta B/B \le 10^{-5}$.

DOI: 10.1134/S001679321508006X

1. INTRODUCTION

The RHESSI data (Lin et al., 2002) make it possible to obtain solar images in hard X rays (HXRs) with a resolution of 5″–15″, which corresponds to approximately 3.6–10.8 Mm. The X-ray brightness distribution along a magnetic loop gives important additional information about the dynamics of the propagation of accelerated electrons and their bremsstrahlung. Coordination of the modeling results with the HXR observations makes it possible to obtain limitations upon the accelerated electron distribution function and the electron angular and energetic distributions. The general problem statement concerning the electron kinetics in plasma with the magnetic field converging to loop footpoints was for the first time formulated in (Hamilton et al., 1990). The next works considered partial processes of Coulomb scattering and magnetic mirroring (Melnikov et al., 2009; Charikov et al., 2012, 2013) with the addition of the reverse current (Zharkova et al., 2010). Kontar et al. (2014) considered the influence of turbulent pitch angle scattering, along with Coulomb collisions, on the accelerated electrons dynamics. However, this work ignores the effects of the magnetic reflection and reverse current; the plasma density is written as a function of altitude z in the Fokker–Planck equation but is set as a constant in the calculations, which does not correspond to the flaring magnetic loop model. In the present work, we tried to take these disadvantages into account and, thereby, to progress in studying the electron beam dynamics in flaring loop plasma and HXR generation.

2. KINETICS OF ACCELERATED ELECTRONS IN FLARING LOOPS

The dynamics of a beam of electrons accelerated during flares is studied by solving the time-dependent relativistic Fokker–Planck equation. This equation takes into account the processes of Coulomb scattering and magnetic mirroring and the effect of the reverse current and magnetic turbulence in magnetic configurations with a specified plasma density and magnetic field induction distributions.

We write the Fokker–Planck equation in the form (Hamilton et al., 1990; Zharkova et al., 2010; Kontar et al., 2014):

$$\begin{aligned}\frac{\partial f}{\partial t} &= -c\beta\mu\frac{\partial f}{\partial s} + c\beta\frac{\partial \ln(B)}{\partial s}\frac{\partial}{\partial \mu}\left[\frac{(1-\mu^2)}{2}f\right] \\ &+ \frac{c}{\lambda_0}\frac{\partial}{\partial E}\left(\frac{f}{\beta}\right) + \frac{c}{\lambda_0\beta^3\gamma^2}\frac{\partial}{\partial \mu}\left[(1-\mu^2)\frac{\partial f}{\partial \mu}\right] \\ &+ \frac{eE^*\beta\mu}{m_e c}\frac{\partial f}{\partial E} + \frac{eE^*(1-\mu^2)}{m_e\beta c}\frac{\partial f}{\partial \mu} \\ &+ \left(\frac{\delta B}{B}\right)^2\frac{c\beta}{2\lambda_B}\frac{\partial}{\partial \mu}\left[|\mu|(1-\mu^2)\frac{\partial f}{\partial \mu}\right] + S(E, \mu, s, t),\end{aligned} \quad (1)$$

where $f(E, \mu, s, t)$ is the accelerated electron distribution function, s is the distance along a field line (counted off from the loop top), t is the current time, $\mu = \cos\alpha$ is pitch angle cosine, $\lambda_0(s) = \dfrac{10^{24}}{n(s)\ln\Lambda}$ cm, $\beta = v\mathrm{s}^{-1}$, v is the accelerated electron velocity, c is the

velocity of light, $\gamma = E + 1$ is the electron Lorentz factor, E is the electron kinetic energy expressed in units of the electron rest energy, and λ_B is the characteristic longitudinal correlation length of magnetic field fluctuations. The reverse compensating current originates when an accelerated electron flux propagates along a magnetic loop. This current is caused by an induced electric field with strength $E^*(s, t) = \frac{j(s,t)}{\sigma(s)} = \frac{e}{\sigma(s)} \int_{E_{\min}}^{E_{\max}} v(E)dE \int_{-1}^{1} f(E, \mu, s, t)\mu d\mu$, where $\sigma(s)$ is the classical Spitzer background plasma conductivity related to Coulomb collisions. We should note that the eddy diffusion coefficient ($D^T_{\mu\mu}$) depends on the form of the magnetic field fluctuation spectrum or the correlation function, which are unknown for solar flares. To estimate the influence of eddy diffusion on the accelerated electron dynamics, we assume the model specification of the correlation function $C(z) \sim \exp(-z/\lambda_B)$. In this case the magnetic fluctuation spectrum takes the form of Lorentzian $W(k_\parallel) = \frac{(\delta B)^2}{\pi} \frac{(1/\lambda_B)}{(1/\lambda_B)^2 + k_\parallel^2}$ (Lee, 1982). In a strong field approximation $v \ll \Omega_{ce}\lambda_B$, where Ω_{ce} is the electron gyrofrequency, the eddy diffusion coefficient can be written as $D^T_{\mu\mu} = 0.5|\mu|(1-\mu^2)\left(\frac{\delta B}{B}\right)^2 \frac{v}{\lambda_B}$. It is evident that the eddy diffusion coefficient is proportional to the electron velocity, and higher-energy electrons are scattered more effectively. In the case of Coulomb scattering, the diffusion coefficient decreases with increasing electron energy and increases with increasing plasma density.

The λ_B value is determined from the strong field condition ($\lambda_B \gg v/\Omega_{ce}$) and depends on the maximal energy of accelerated electrons and the magnetic field in a loop (the minimal value in a loop is taken). For the parameters used in this work, λ_B is approximately 10^2 cm. An increase in λ_B (e.g., for rather high loops where the magnetic field induction at the top is only (5–15) G) will result in a decrease in the role of electron scattering by magnetic field inhomogeneities. In this case the effects related to magnetic turbulence described below can take place but at a larger $\eta = \delta B/B$ value. The mean free path of accelerated electrons, related to scattering by magnetic fluctuations and ambient plasma ions, can be calculated by the formula $\lambda = \frac{3v}{8} \int_{-1}^{1} \frac{(1-\mu^2)^2}{D^T_{\mu\mu} + D^C_{\mu\mu}} d\mu$, where $D^C_{\mu\mu}$ is the Coulomb diffusion coefficient. The path length related to Coulomb interactions is $\lambda^C \sim 10^{10}$ cm for 30-keV electrons at a loop top, which is larger than the path length related to turbulent scattering ($\lambda^T \sim 10^9$ cm) at $\eta = \delta B/B = 10^{-3}$ by an order of magnitude. At a loop footpoint, λ^C is smaller by three to five orders of magnitude λ^T, as a result of which Coulomb diffusion completely predominates in corresponding loop zones. In intermediate loop zones between a top and footpoints, where the ambient plasma density is $n_e \sim 10^{11}$ cm^{-3}, path lengths λ^T and λ^C are commensurable ($\lambda^T \sim \lambda^C$).

The plasma density distribution along a loop is specified phenomenologically based on RHESSI observations in the chromosphere $n_e = 1.25 \times 10^{13}(z/1\ \text{Mm})^{-2.5}$ cm^{-3}, where z is altitude. The plasma density in the loop coronal area has been studied less thoroughly and may also be variable due to evaporation during the flare impulsive phase. Nevertheless, at altitudes of $z \sim 10$–20 Mm in the corona, this formula gives plasma density values that agree with different theoretical values and observations (Aschwanden, 2002).

The magnetic field distribution in a loop is even more uncertain and is only specified based on the field induction convergence toward loop footpoints. The previous works (e.g., (Hamilton et al., 1990; Melnikov et al., 2009; Zharkova et al., 2010; Charikov et al., 2012)) took into account only the magnetic field induction component along the s axis dependent on coordinate s. A convergent magnetic field is evidently not homogeneous, and the Maxwell equation (Div$\mathbf{B} = 0$) is not fulfilled rigorously at such a magnetic field induction specification. Therefore, for a one-dimensional problem with respect to coordinate, it is necessary to assume that the magnetic field convergence should be weak and the field line curvature is insignificant. Consequently, we accepted that the ratio of the induction at a loop footpoint to its value at a top ($B_{\max}/B_0$) is 2 for most variants. We specify a model magnetic field converging toward loop footpoints according to (McClements, 1992) in the form: $\frac{B(s)}{B_0} = 1 + \frac{(s-b_1)^2}{h_b^2}$, where $B_0 = 100$ G is the minimal magnetic field value, and b_1 specifies the spatial shift of the magnetic field minimum from the loop geometric top. The $B_{\max}/B_0$ ratio varied and was taken to be equal to 2 in most models. The characteristic scale of magnetic field variations (h_b) is determined based on the specified $B_{\max}/B_0$ ratio and b_1 value. The last term in (1) specifies the distribution of accelerated electrons during their injection. During this period, the functional dependence of the accelerated electron source on arguments is represented in the factorized form; i.e., it is assumed that the processes resulting in the formation of such a distribution function during the electron acceleration $S(E, \alpha, s, t) = KS_1(E)S_2(\alpha)S_3(s)S_4(t)$, where $K = (10^6$–$10^7)$ cm^{-3} s^{-1} is the normalization factor, are independent. The electron energy spectrum in a source is power with index $\delta = 3$. Cases of an isotropic injection ($S_2(\alpha) = 1$) and an anisotropic electron distribution along the magnetic field in a certain pitch angle cone ($S_2(\alpha) = \cos^6(\alpha)$ and $S_2(\alpha) = \exp(-(\alpha - \alpha_1)^2/\alpha_0^2)$, $\alpha_1 = 0°$,

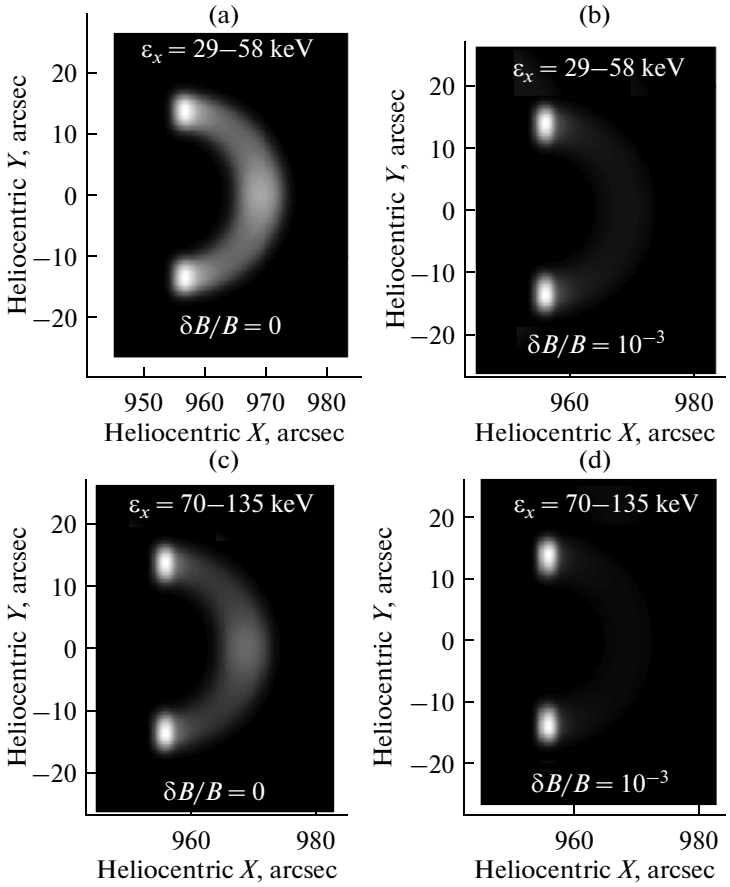

Fig. 1. HXR distribution at an injection maximum along a magnetic loop in two energy ranges (ε_x = 29–58 (top) and 70–135 (bottom) keV, respectively) for the model of injection with an isotropic electron source, ignoring turbulence (1a, 1c) and with regard to scattering by magnetic inhomogeneities with $\delta B/B = 10^{-3}$ (1b, 1d). A magnetic loop is located at the solar limb. The figure corresponds to the injection maximum time.

$\alpha_0 = 35.9°$) are considered. Accelerated electrons are injected in the upper loop zone. The time profile during injection is an isolated pulse in the Gaussian form with a characteristic pulse width of 1.4 s.

The HXR intensity is calculated according to the relativistic bremsstrahlung formulas (Gluckstern and Hull, 1953; Bai and Ramaty, 1978). In contrast to numerous previous works on HXR calculation, we take into account an actual magnetic loop position on the solar disk, according to which HXRs are calculated at each loop point at a local observation angle, and the loop geometric volume is taken into account. For model calculations, the loop section is a semicircle with a center at a distance of 955 arcsec from the solar disk center along the horizontal heliocentric axis and 0 arcsec along the vertical axis.

3. INFLUENCE OF MAGNETIC TURBULENCE ON THE HXR BRIGHTNESS DISTRIBUTION

We consider the calculated HXR distribution along a magnetic loop. Figure 1 presents the spatial distribution of HXRs with energies of 29–58 and 70–135 keV for the electron injection maximum instant for a model in which the electron source during injection is isotropic and magnetic turbulence is absent $\delta B/B = 0$ (panels 1a, 1c) and is taken into account $\delta B/B = 10^{-3}$ (panels 1b, 1d). When turbulence is absent (left-hand panels), the HXR brightness distribution has three sources: less HXR contrast at the top and more intense HXR at loop footpoints. A similar HXR brightness distribution was previously referred to in several works (e.g., (Charikov et al., 2012)) and is related to the accumulation of electrons with pitch angles close to 90° at the top, because electrons with small pitch angles escape into loss cone. As was mentioned above, higher-energy electron Coulomb scattering becomes less effective, as a result of which these electrons accumulate less intensely at a loop top. Therefore, the brightness of HXRs with energies of 70–135 keV at the loop top is small as compared to the brightness of footpoints (Fig. 1c); for lower energies, the contrast decreases (Fig. 1a). We consider the influence of accelerated electron scattering by homogeneous magnetic turbulence along a loop with $\eta = \delta B/B = 10^{-3}$. The X-ray source at the loop top becomes less bright as com-

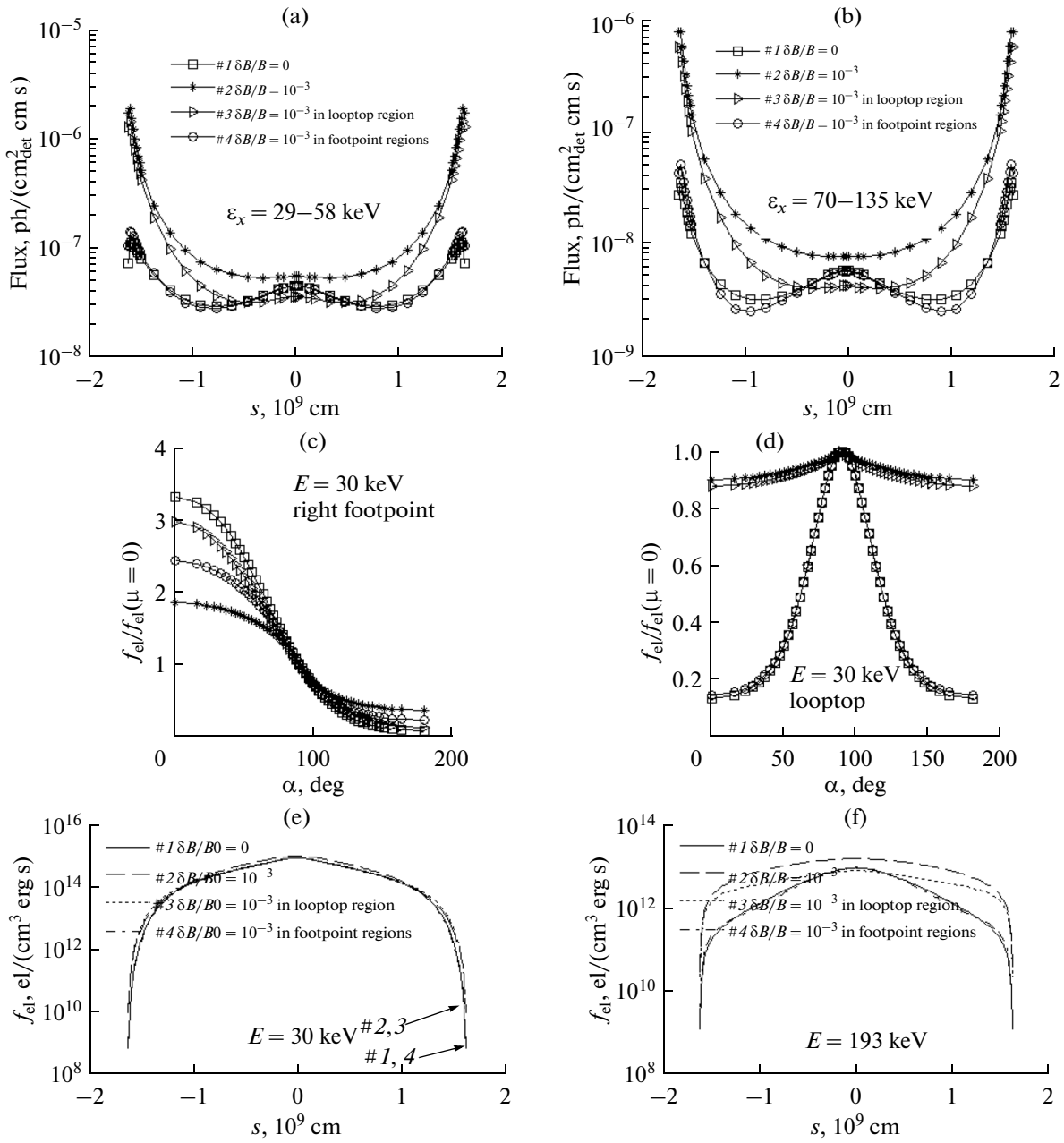

Fig. 2. Panels (a) and (b) present the HXR distribution at energies of $\varepsilon_x = 29–58$ and 70–135 keV integrated over the cross section: magnetic turbulence is absent (curve *1*), is uniformly distributed along a loop (*2*), and is localized at the loop top (*3*) and footpoints (*4*). Panels (c) and (d) show the angular dependence of the electron distribution function, which is differential with respect to the energy and is integrated over a rather wide loop area at its top (d) and footpoint (c). The electron distribution function is normalized to its value when the pitch angle is $\alpha = 90°$. The curve denotations in Figs. 2c and 2d coincide with the denotations in Figs. 2a and 2b. Panels 2e and 2f show the electron distribution functions along a loop for electron energies of $E = 30$ and 193 keV. The electron source is isotropic ($S(\alpha) = 1$). The figure corresponds to the injection maximum time.

pared to HXRs from footpoints, especially at high energies (see Figs. 1b, 1d).

Besides the case of magnetic turbulence uniformly distributed along a loop, we considered situations in which magnetic turbulence is localized at a top with an injection characteristic scale of $s_0^{turb} = 1e + 9$ cm and at loop footpoints with $s_0^{turb} = 0.4e + 9$ cm. The calculations are illustrated in Fig. 2 for the distributions integrated over a loop cross section.

Figures 2a and 2b show that the footpoint brightness increases by a factor of ~2 of magnitude for 29–58 keV HXRs and slightly more strongly for 70–135 keV quanta, if homogeneous magnetic turbulence

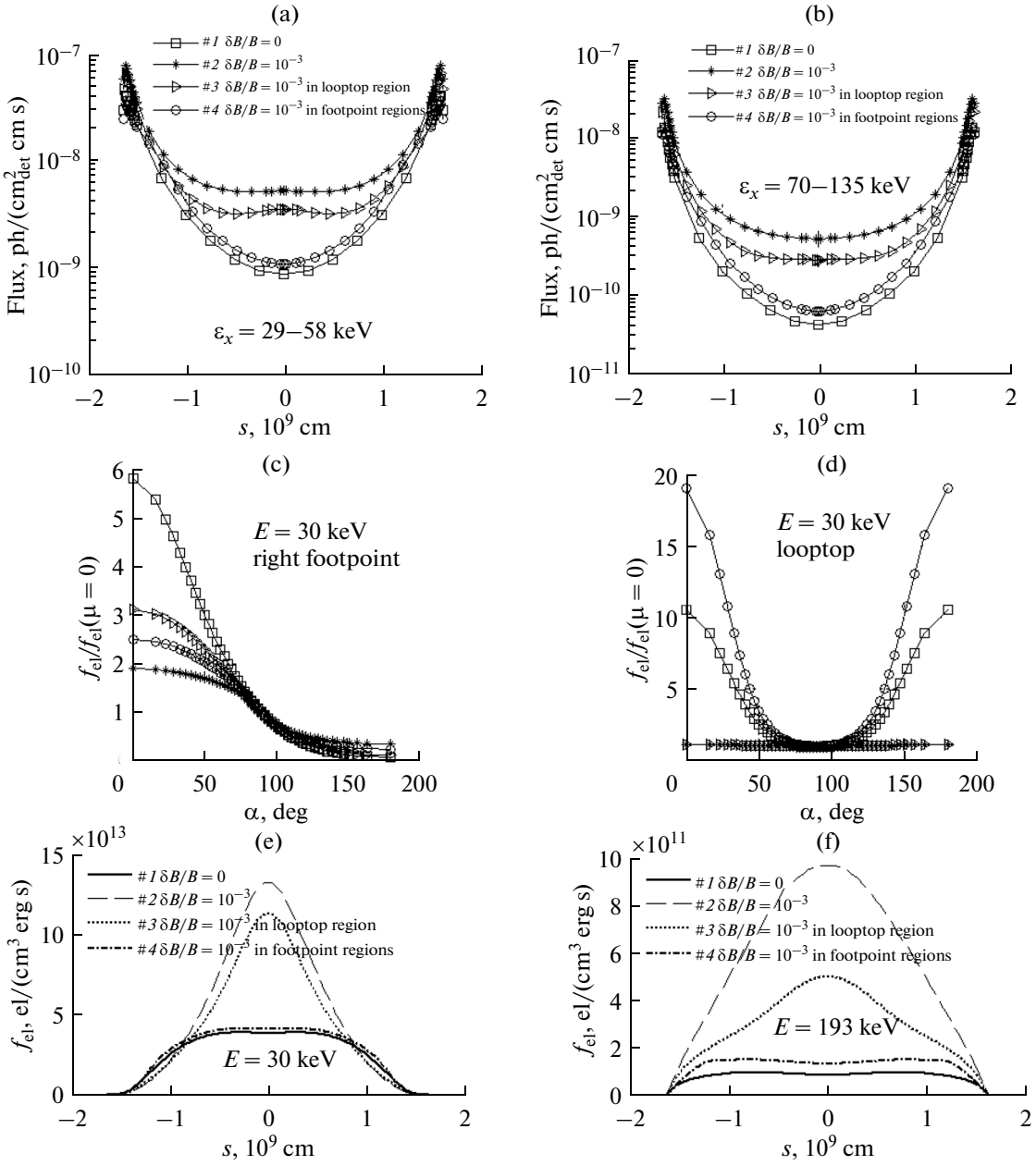

Fig. 3. The same as in Fig. 2 but for an anisotropic electron injection at $S(\alpha) = \cos^6(\alpha)$.

and magnetic turbulence localized at a loop top with $\eta = \delta B/B = 10^{-3}$ are taken into account (see curves *2* and *3* as compared to curve *1*). The HXR distribution at a loop top is different. In a model with magnetic turbulence localized at a loop top, the HXR intensity is slightly lower (Figs. 2a, 2b; curves *3*) than in a model with only Coulomb scattering (curves *1*) independently of the energy. Similar HXR distributions are related to the fact that electrons escape from a loop top as a result of more effective scattering (Figs. 2e, 2f; curves *3*). In the intermediate zone between the loop top and footpoint and at footpoints (Figs. 2e, 2f), the number of trapped electrons increases due to electron isotropization with respect to the pitch angles in the presence of magnetic turbulence (Figs. 2c, 2d). However, if turbulence is present in the entire loop, an inverse process proceeds at loop footpoints: the number of electrons with pitch angles along the magnetic field decreases, which results in increased particle trapping (see Fig. 2c). A generally larger number of electrons in the intermediate zone between the loop top and footpont at an injection maximum instant results in an increased number of electrons in regions where the background plasma density is higher, which in turn results in an increase in the HXR brightness at loop footpoints.

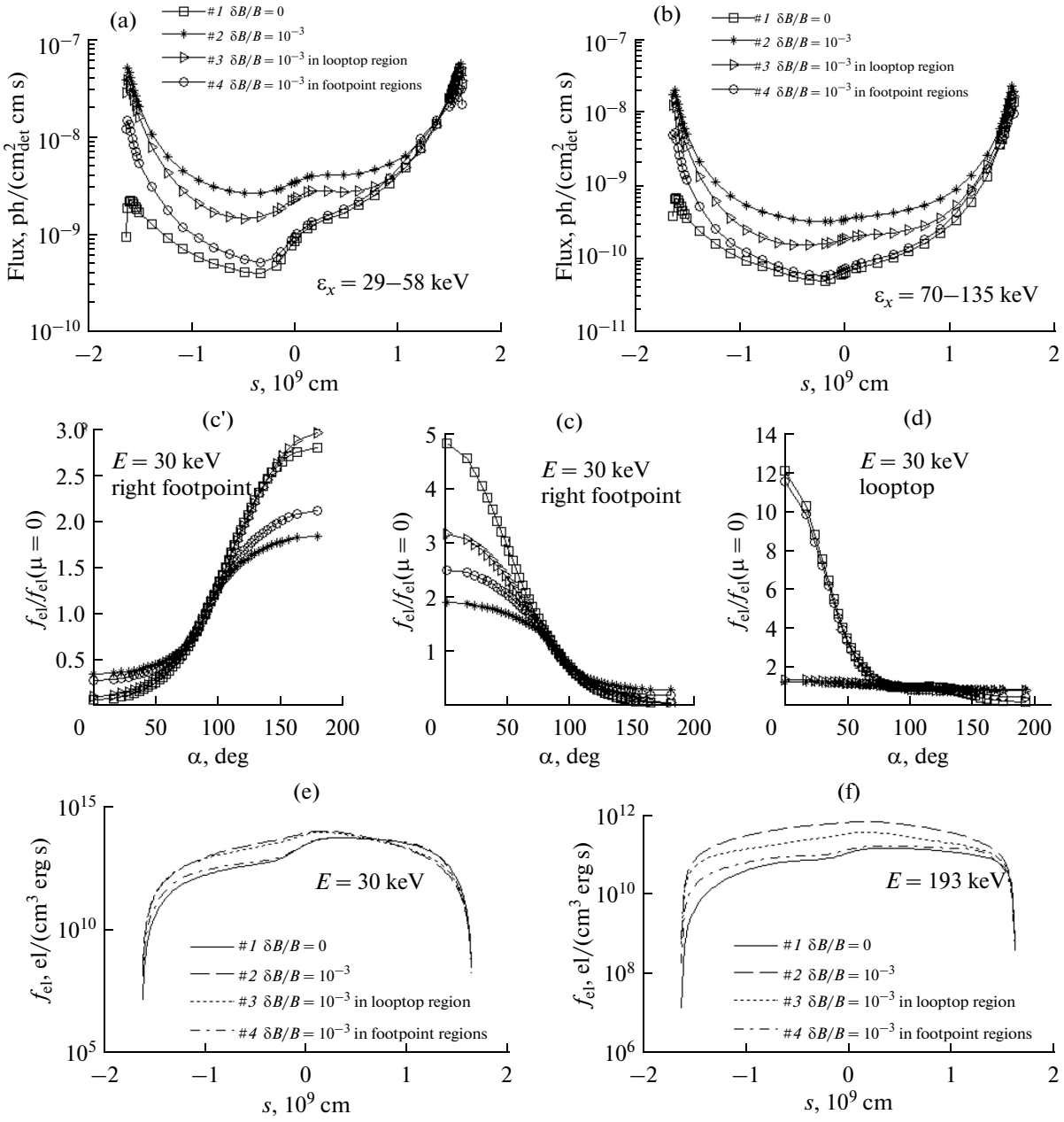

Fig. 4. The same as in Fig. 2 but for an anisotropic electron injection at $S_2(\alpha) = \exp(-(\alpha - \alpha_1)^2/\alpha_0^2)$, $\alpha_1 = 0°$, and $\alpha_0 = 35.9°$.

When turbulence is localized at the footpoints (see Figs. 2a, 2b; plot 4), this does not result in substantial changes in the HXR brightness distribution, because the effect of Coulomb collisions is predominant in this region, where the ambient cold plasma density is higher than the plasma density in the coronal loop part by two to five orders of magnitude.

We consider the results of the calculations in the anisotropic models.

Figure 3 shows curves, which are similar to those presented in Fig. 2, for an anisotropic source $S(\alpha) = \cos^6(\alpha)$. According to such a model angular distribution, electrons are accelerated symmetrically about the magnetic field and the direction is most probably related to the electric field vector. The electron isotropization (see the curves in panels 3c, 3d) and, as a consequence, a substantial electron accumulation in the coronal loop part (see panels 3e, 3f) result in increased brightness along the entire loop, but especially at a loop top (by a factor of ~4), as well as in the anisotropic case, when magnetic turbulence is distributed uniformly and is localized at a top (see panels 3a, 3b; curves *1*–*3*). As in the isotropic case, the localization

of magnetic turbulence at footpoints insignificantly affects the HXR distribution (see panels 3a, 3b; curve *4*).

Figure 4 shows curves, which are similar to those presented in Fig. 2, for an anisotropic source with the injection angular function $S_2(\alpha) = \exp(-(\alpha - \alpha_1)^2/\alpha_0^2)$, $\alpha_1 = 0°$, $\alpha_0 = 35.9°$. The function corresponds to an injection toward the "right" footpoint (positive *s*). Panels 4a and 4b show that the presence of turbulence in the entire loop or at its top results in a substantial increase in the HXR brightness in the coronal loop part and at footpoints, which is the opposite of the injection direction (see curves *1–3*). In contrast to the previous cases, when turbulence is present at footpoints (see curve *4*), this results in a considerable increase in HXR brightness at the "left" loop footpoint. In all cases the increase in the HXR brightness results from the isotropization of electrons that fly toward the chromosphere and fall in a magnetic trap (see panels 4c', 4c, 4d). Panels 4e and 4f indicate that electrons are intensely accumulated at the loop top and left footpoint, if turbulence is present in the entire loop or at its top (see curves *2*, *3* as compared to curve *1*). However, the presence of turbulence only at footpoints in this model caused electrons to accumulate mostly in the left half-loop, as a result of which the left footpoint was rather bright (see Panels 4e, 4f; curves *4* as compared to curve *1*).

4. CONCLUSIONS

We indicated that the HXR intensity substantially increases at the electron injection maximum at loop footpoints and in the coronal part when a source is isotropic and anisotropic $S(\alpha) = \cos^6(\alpha)$, respectively, if magnetic turbulence is present in a flaring loop ($\eta = \delta B/B = 10^{-3}$). In the isotropic case, HXRs intensify in the intermediate zone between the loop top and footpoint also but more weakly than at footpoints. In a model with magnetic turbulence localized at a loop top, the HXR intensity at the top is lower (for an isotropic model) than in a model with Coulomb scattering, which is related to the fact that magnetic turbulence is mainly effective only in a region with low ambient plasma density, where Coulomb effects are weak. The latter circumstance is also confirmed by curve *4* in Figs. 2a, 2b, 3a, and 3b, when turbulence was present only at loop footpoints. However, we should be careful, since turbulence at footpoints is so effective that it can qualitatively change the HXR distribution along a loop in the case of an asymmetric source (see Figs. 4a, 4b; curves *4*). In all cases a change in HXR brightness mostly results from the electron isotropization in the pitch angle space. In most cases isotropization results in an increase in the number of trapped electrons, especially in anisotropic cases. This leads to an increase in the HXR brightness in the loop coronal and intermediate parts in anisotropic and isotropic models, respectively. The HXR brightness distribution in isotropic and anisotropic models is different, because electron isotropization at a top results not only in a decrease in the number of electrons in this region in the isotropic case, when turbulence is present in the entire loop for example (since the electron transverse pulse distribution changes into the isotropic distribution), but also in the trapping of electrons in the intermediate region (since the electron longitudinal pulse distribution changes into the isotropic distribution, and the contribution of electrons with pitch angles about 90° increases). At the same time, in the anisotropic case, the electron pitch angle distribution at a top is quasi-longitudinal rather than quasi-transverse as in the isotropic case. Therefore, in an anisotropic model, electron isotropization results in increased electron trapping at the top and in the loop intermediate part.

Thus, in all cases the presence of turbulence results in an increase in the HXR brightness at footpoints and at a loop top, mainly in isotropic and anisotropic models, respectively. In asymmetric models brightening at the loop top and footpoints can differ depending on the degree of the electron angular distribution asymmetry in an injector. A similar influence of magnetic turbulence takes place for a sufficiently high values of parameter $\eta = \delta B/B = 10^{-3}$. As η decreases, the role of scattering by inhomogeneities decreases and becomes insignificant at $\delta B/B \le 10^{-5}$.

ACKNOWLEDGMENTS

A.N. Shabalin was partially supported by the Russian Foundation for Basic Research (project no. 14-02-00924) and by the presidium of the Russian Academy of Sciences (program 9).

REFERENCES

Aschwanden, M.J., Brown, J.C., and Kontar, E.P., Chromospheric height and density measurements in a solar flare observed with RHESSI-II. Data analysis, *Sol. Phys.*, 2002, vol. 210, pp. 383–405.

Bai, T. and Ramaty, R., Backscatter, anisotropy, and polarization of solar hard X-rays, *Astrophys. J.*, 1978, vol. 219, pp. 705–726.

Charikov, Yu.E., Melnikov, V.F., and Kudryavtsev, I.V., Intensity and polarization of the hard X-ray radiation of solar flares at the top and footpoints of a magnetic loop, *Geomagn. Aeron.* (Engl. Transl.), 2012, vol. 52, pp. 1021–1031.

Charikov, Yu.E., Shabalin, A.N., and Kudryavtsev, I.V., Hard X-ray emission of accelerated electrons in a loop-structure of the magnetic field during solar flares, *Nauchno-Tekh. Vedomosti SPbGPU. Fiz-Mat. Nauki*, 2013, no. 4-1, pp. 154–165.

Gluckstern, R.L. and Hull, M.H., Polarization dependence of the integrated bremsstrahlung cross section, *Phys. Rev.*, 1953, vol. 90, no. 6, pp. 1030–1035.

Hamilton, R.J., Lu, E.T., and Petrosian, V., Numerical solution of the time-dependent kinetic equation for electrons in magnetized plasma, *Astrophys. J.*, 1990, vol. 354, pp. 726–734.

Kontar, E.P., Bian, N.H., Emslie, A.G., and Vilmer, N., Turbulent pitch-angle scattering and diffusive transport of hard-X-ray producing electrons in flaring coronal loops, *Astrophys. J.*, 2014, vol. 780, no. 2, 176.

Lee, M.A., Coupled hydromagnetic wave excitation and ion acceleration upstream of the Earth's bow shock, *J. Geophys. Res.*, 1982, vol. 87, no. A7, pp. 5063–5083.

Lin, R.P., Dennis, B.R., Hurford, G.J., et al., The Reuven Ramaty Righ-Energy Solar Spectroscopic Imager (RHESSI), *Sol. Phys.*, 2002, vol. 210, no. 3.

McClements, K.G., The simultaneous effects of collisions, reverse currents and magnetic trapping on the temporal evolution of energetic electrons in a flaring coronal loop, *Astron. Astrophys.*, 1992, vol. 258, pp. 542–548.

Melnikov, V.F., Gorbikov, S.P., and Pyatakov, N.P., Formation of anisotropic distributions of mildly relativistic electrons in flaring loops, *Universal Heliophysical Processes, Proceedings of IAU Symposium 2008, No. 257*, Gopalswamy, N. and Webb, D. F., Eds., 2009, pp. 323–328.

Zharkova, V.V., Kuznetsov, A.A., and Siversky, T.V., Diagnostics of energetic electrons with anisotropic distributions in solar flares-I. Hard X-rays bremsstrahlung emission, *Astron. Astrophys.*, 2010, vol. 512, A8.

Translated by Yu. Safronov